Cement and Concrete Composites 134 (2022) 104792

Contents lists available at ScienceDirect

Cement and Concrete Composites

journal homepage: www.elsevier.com/locate/cemconcomp

Portland cement hydration in the vicinity of electrically polarized conductive surfaces

Kamila Gawel *, Sigurd Wenner, Narjes Jafariesfad, Malin Torsæter, Harald Justnes

SINTEF Industry, SP Andersens Veg 15b, 7031, Trondheim, Norway

ARTICLE INFO

Keywords:
Portland cement
Hydration
Electrical polarization
Hydration products
Surface
Steel
Graphite

ABSTRACT

Hardening of Portland cement-based materials in vicinity of electrically conductive surfaces, especially when the surfaces are electrically or galvanically polarized, can lead to both morphological and chemical changes in cement close to the surfaces due to combined electrochemical and electrophysical processes.

Cement hydration products close to graphite and steel surfaces being positively (anode) and negatively (cathode) electrically polarized (direct current) were studied. Scanning Electron Microscopy and Energy Dispersive X-ray Spectroscopy were used to compare structure and atomic composition of cement hydration products on cathode, anode and a reference surface with no electrical polarization.

The application of direct current (DC) potential in aqueous Portland G cement dispersion significantly affects cement hydration products close to cathode and anode and different products were found at the anode compared to the cathode surfaces. At the graphite anode, calcium sulphate crystals along with calcium hydroxide were most abundant, while the graphite cathode was mainly covered with calcium hydroxide. The calcium hydroxide carbonated upon exposure to air during drying. When steel electrodes where used, the most significant adsorption occurred at the anode, in contrast to graphite where the largest amount of the adsorbed material was found on the cathode. The observed differences were explained in view of electrophysical (electrophoresis, electroosmosis) and electrochemical (reduction and oxidation) processes occurring at electrode surfaces upon application of DC current.

The knowledge gained in this work is important for engineering of electrically conductive cement nanocomposites where typically the contact surface of an electrically conductive filler and a cementitious matrix is high.

1. Introduction

Hydration of Portland cement is a process in which clinker minerals and gypsum react with water to form solid hydrates. In this way, Portland cement-based materials like cement pastes, concretes, mortars, and cement composites are gaining the mechanical strength necessary for the application of these materials in construction [1]. It relies on reactions of anhydrous calcium silicates, calcium aluminates and calcium aluminoferrites with water [2]. The hydration reactions lead to the formation of amorphous calcium silicate hydrate gel (C–S–H), acting as a glue, and crystalline calcium hydroxide as the main hydration products [3].

The conditions under which the hydration occurs play a crucial role in the development of microstructure of cement-based materials and thus affect the properties of the resulting hardened materials [1]. The parameters like temperature [4], pressure [5], and concentration of different additives have been broadly utilized to engineer the cement hydration. Much less is however known about how the electric field and electrical polarization affect the hydration of Portland cement. Especially nowadays, when electrically conductive cement composites are under development, knowledge on how electric fields may affect cement hydration and the resulting material properties is of paramount importance. The effect of electric fields on the final material (hardened cement paste) is also of high interest.

It has been shown that application of alternating current (AC) to the hardening cement mortar/carbon nanofiber composite causes heating due to electrical resistance that can be applied to accelerate cement hardening/hydration [6,7]. Such heating of hardening cement materials was suggested to be utilized for cementing in permafrost and or at low temperatures, where freezing of hardening cement-based structures is

* Corresponding author.
E-mail address: kamila.gawel@sintef.no (K. Gawel).

https://doi.org/10.1016/j.cemconcomp.2022.104792
Received 22 October 2021; Received in revised form 18 February 2022; Accepted 26 September 2022
Available online 7 October 2022

Table 1
Composition of Portland cement class G given by the supplier.

	SO_3	Free lime	SiO_2	Al_2O_3	Fe_2O_3	CaO	MgO	P_2O_5	K_2O	Na_2O
wt %	2.01	0.62	21.82	4.00	5.45	63.60	1.57	0.05	0.34	0.29

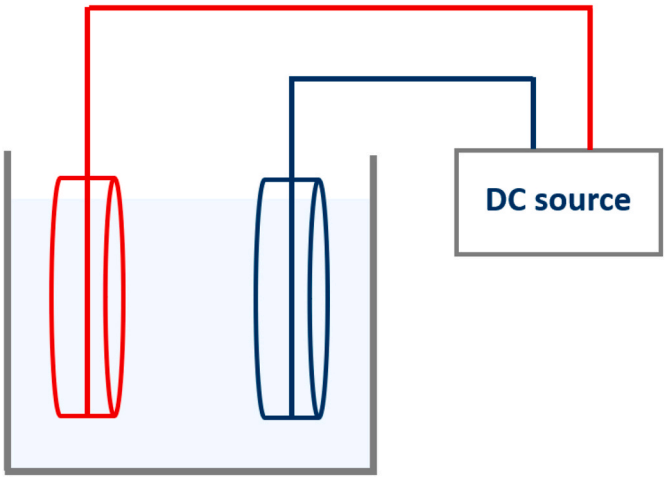

Fig. 1. Schematic illustration of the experimental setup.

destructive for the construction [8]. In fact the electrical resistance heating of cement materials (without electrically conductive fillers) as a way to accelerate curing was proposed already in the 1940s [9]. Compositional and structural differences between the same materials cured at room temperature and AC treated have been investigated [7] showing that electrically heated cement contains larger amount of hydration products at early stage as an indication of accelerated hydration.

Ding et al. have shown that electrical polarization of cement-based piezoelectric composites at the early stage of hardening significantly affects the structure of the main cement hydration product calcium silicate hydrate (CSH) phase [10,11]. More specifically, the CSH gel morphology changed from fibrous to ellipsoid after polarization at high temperatures.

Lavrov et al. applied DC current during hardening of Portland G cement to engineer cement structure in the vicinity of electrically conductive pipes [12–14]. They reported significant morphological changes close to the steel pipes constituting cathode and anode [14]. The morphological changes had an effect on the shear forces between the steel pipes and the surrounding cement paste matrix [13]. It has been suggested that combined electrophysical (electrophoresis, electroosmosis) and electrochemical (oxidation and reduction reactions) influences the microstructure of hardened cement pastes close to electrodes. However, an explanation is still warranted on how the above-mentioned processes affect cement hydration and what is the difference in cement hydration products in cement bulk compared to electrode surfaces. This paper aims on filling in this knowledge gap.

The goal of this work was to characterize Portland G cement hydration products in the vicinity of electrically polarized conductive surfaces. Two types of surface materials were used in the study: (1) inert graphite that does not undergo corrosion when anodically polarized and (2) steel that under electric or galvanic polarization will undergo anodic corrosion. Scanning Electron Microscopy (SEM) and Energy Dispersive X-ray Spectroscopy (EDS) were used to characterize the cement hydration products deposited from diluted cement slurry.

2. Materials and methods

2.1. Preparation of cement suspension

40 g of Portland cement class G from Norcem (Norway) with composition given by the supplier and presented in Table 1 was mixed with 240 ml of fluid (2-propanol (VWR) or distilled water). The mixture was stirred for 3 min using a magnetic stirrer before the electrodes were immersed in the slurry and the potential was switched on. The aim of using 2-propanol was two-fold: (1) to avoid cement particles hydration so that only partitioning of unhydrated cement particles between electrodes take place in electric field (2) to allow only electric field (2-propanol is a dielectric fluid) and exclude pH changing electrochemical processes that otherwise occur in water.

2.2. Electrical polarization

Fig. 1 presents a schematic illustration of the experimental setup consisted of: (1) a beaker with the cement slurry; (2) electrodes (cathode and anode) made of either graphite or carbon steel; (3) DC power supply.

The electrodes were immersed in the cement slurry 3 min after the slurry was prepared. The potential at the DC source was set at 10 V. 10 V was chosen to ensure that electric field in dielectric fluid as 2-propanol will be strong enough to allow for the separation of differently charged particles. The slurry was stirred with a magnetic stirrer for the next 6 min whereafter stirring was turned off so that the particles not adsorbed at electrodes could settle under gravity. The slurry was left to sediment under gravity control for the next 2 min. After 8 min (in total) of surface polarization in the slurry, the potential was switched off and the electrodes were removed from the solution. The excess of the solution residing at the bottom edge of the electrode was removed. Next the electrodes with adsorbed particles were cured in air at ambient conditions for 10 h before they were placed in a sealed containers to avoid further reactions of cement hydration products with CO_2 from air before SEM and EDS measurements. It is expected that electrode surface and adsorbed particles drying was relatively quick process (the surface seemed dry (free for water) already after couple of minutes (2-propanol drying was even faster). Nevertheless, as carbonation is rather quick process some carbonation of hydration products before the surface is completely dry, can not be excluded. Sometimes, to stop hydration processes solvent exchange is used, i.e. water is exchanged to e.g. an alcohol. The authors chosen not to expose deposits to alcohols at the end of water exposure (and instead let the surface dry) to avoid any potential abrasive forces on the surface that could damage/change deposit morphology.

2.3. SEM/EDS characterization of hydration products

Electrodes were imaged with a Hitachi S–3400 N SEM instrument in secondary electron mode, using a voltage of 20 kV and working distance of 10 mm. No coating or other pre-treatment was applied. All imaging and mapping were done at the centre of the electrodes for consistency. Rectangular areas of 0.01 mm^2 were mapped with an Oxford X-MAX 80 EDS detector and a high-current beam. The summed spectra from the areas were quantified using Oxford Aztec.

2.4. Powder X-ray diffraction

Powder XRD pattern was collected using D8 Focus diffractometer

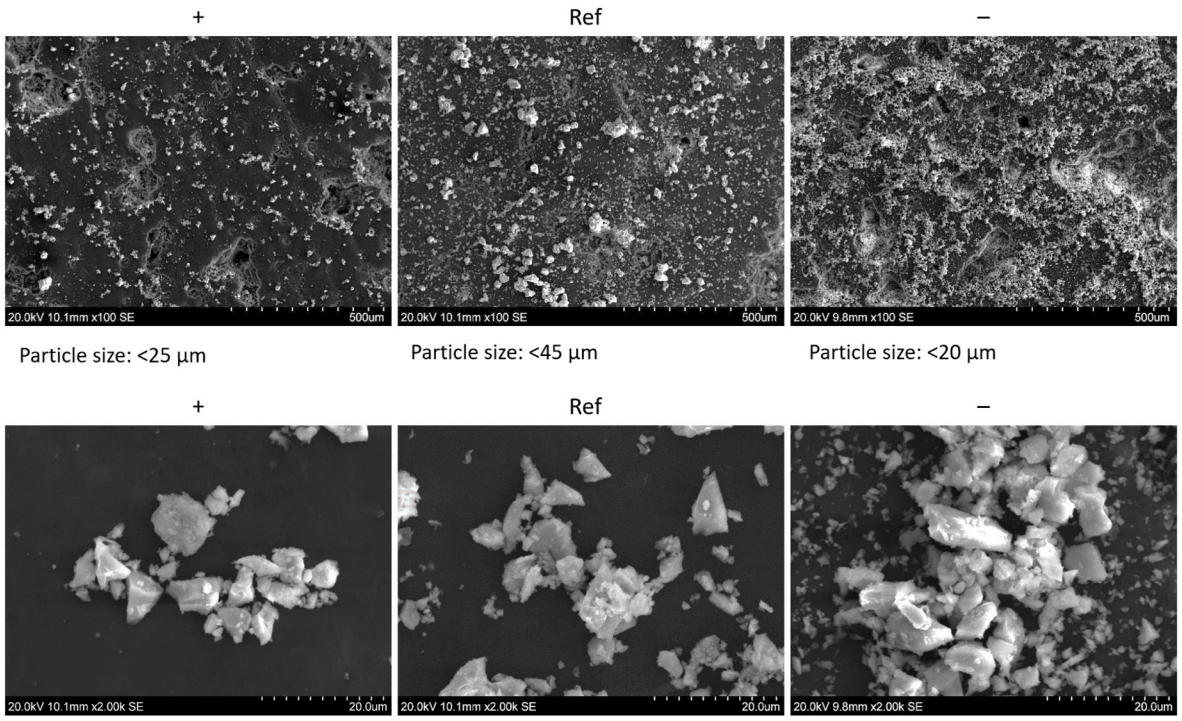

Fig. 2. SEM SE image of the graphite surfaces, anode (+), cathode (-) and the reference surface (R), after removal from the cement dispersion in 2-propanol at two different magnifications. The smaller magnification images are representative for particle size distribution while the larger magnification images show particle shape.

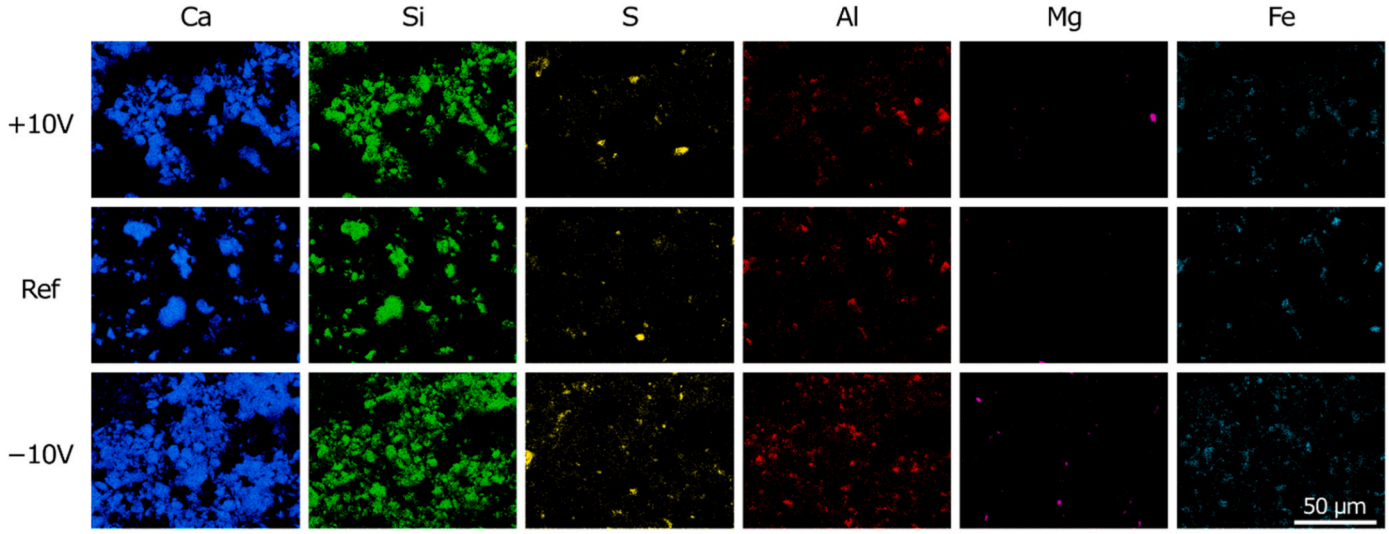

Fig. 3. EDS maps showing elemental composition of cement particles residing on graphite surfaces: anode (+), cathode (-) and the reference surface (Ref), after removal from the cement dispersion in 2-propanol.

from Bruker with a Bragg-Brentano θ–2θ geometry and a goniometer radius of 200.5 mm. The patterns were measured between 3° and 80° 2θ angle with a step size of 0.012°2θ and a sampling time of 0.4 s per step. Co-Kα radiation with a wavelength of approx. 1.79 Å was used as the X-ray source. Crystalline phases were identified using DIFFRAC.EVA V4.0 software (Bruker).

Table 2
Atomic composition of particles present on electrodes (cathode and anode) as well as the reference sample surface after exposure to cement slurry in 2-propanol after 8 min of polarization at 10 V.

at.%	Ca	Si	Al	Fe	Mg	S	Na	P	Cl	K	V	Mn	Ca/Si
+	63.99	19.06	4.55	4.09	3.46	2.52	0.89	0.07	0.15	0.64	0.05	0.53	3.3
ref	63.68	20.34	4.41	4.02	2.83	2.27	1.16	0.00	0.08	0.59	0.07	0.55	3.1
–	64.05	18.69	4.19	4.44	3.24	2.61	0.89	0.22	0.08	0.71	0.31	0.57	3.4

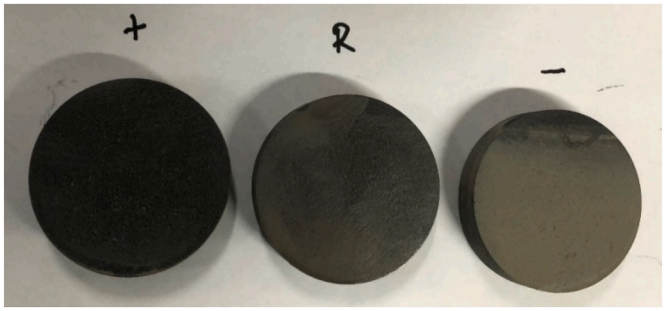

Fig. 4. Photography of graphite electrodes: anode (+), cathode (-) and the reference surface (R) after removal from the cement dispersion in water.

3. Results

3.1. Graphite electrodes in 2-propanol

Fig. 2 presents SEM secondary electron (SE) image of the graphite surfaces, anode (+), cathode (-) and the graphite reference surface with no electrical potential applied (Ref), after removal from the cement dispersion in 2-propanol. The negative electrode attracted the highest amount of particles while the smallest amount was observed on the anode. Particles deposited on all the three surfaces had similar morphology, characteristic for cement particles. All the three electrodes contained particles down to 0.3 μm and smaller. The largest particles were deposited on the reference surface. Energy dispersive X-ray spectroscopy data shown in Fig. 3 and the atomic composition data shown in Table 2 suggest that there are no significant compositional differences between the particles at the three surfaces, since the cement is not hydrating nor reacting with 2-propanol.

EDS maps from the three electrodes are shown in Fig. 3. The summed spectra from the maps were quantified in atomic fraction, as shown in Table 2. Carbon was deconvoluted from the results as the substrate is pure carbon. No large differences in particle chemistry were found between the three surfaces. Judging by the Ca/Si ratio, most particles are tricalcium silicate, as expected.

3.2. Graphite electrodes in water

With water as a dispersion medium, the negative electrode attracts the highest amount of particles, similar to the case of 2-propanol. This can be observed visually in Fig. 4. SEM images of the surfaces are shown in Fig. 5, and corresponding EDS maps are shown in Fig. 6, while atomic composition of particles at electrode surfaces are presented in Table 3. The particle sizes are similar on the three surfaces (cathode, anode and reference) but there are significant differences in the morphology and chemical composition of the particles deposited at the three different surfaces. The particles deposited at the reference surface had similar shape to particles deposited from 2-propanol (non-hydrated cement particles) but in addition there were visible hydration products, in the form of deposits on the surface of the particles. The presence of large amounts of non-hydrated Ca_3SiO_5 particles (or hydrated only at the surface) was confirmed by EDS data (Fig. 7, red circle #3). The deposits present on the negative electrode (cathode) had a fibrillar form, and were identified by EDS as calcium hydroxide (the second most abundant hydration product by mass of Portland G cement after C–S–H) possibly to some extend carbonated ($CaCO_3$). EDS does not unequivocally distinguish between calcium hydroxide and calcium carbonate however the fibrillar rosett morphology may indicate the presence of aragonite [15–17].The material present at the positive electrode (anode) was identified as a mixture of calcium sulphate crystals and calcium hydroxide/calcium carbonate.

3.3. Steel electrodes in water

The most striking difference in adsorption between steel and graphite electrodes in water is the presence of the largest amount of deposit at the positive electrode (anode) rather than the negative electrode in case of steel, as seen in Fig. 8. The deposited material is of greenish colour suggesting the presence of divalent iron compounds.

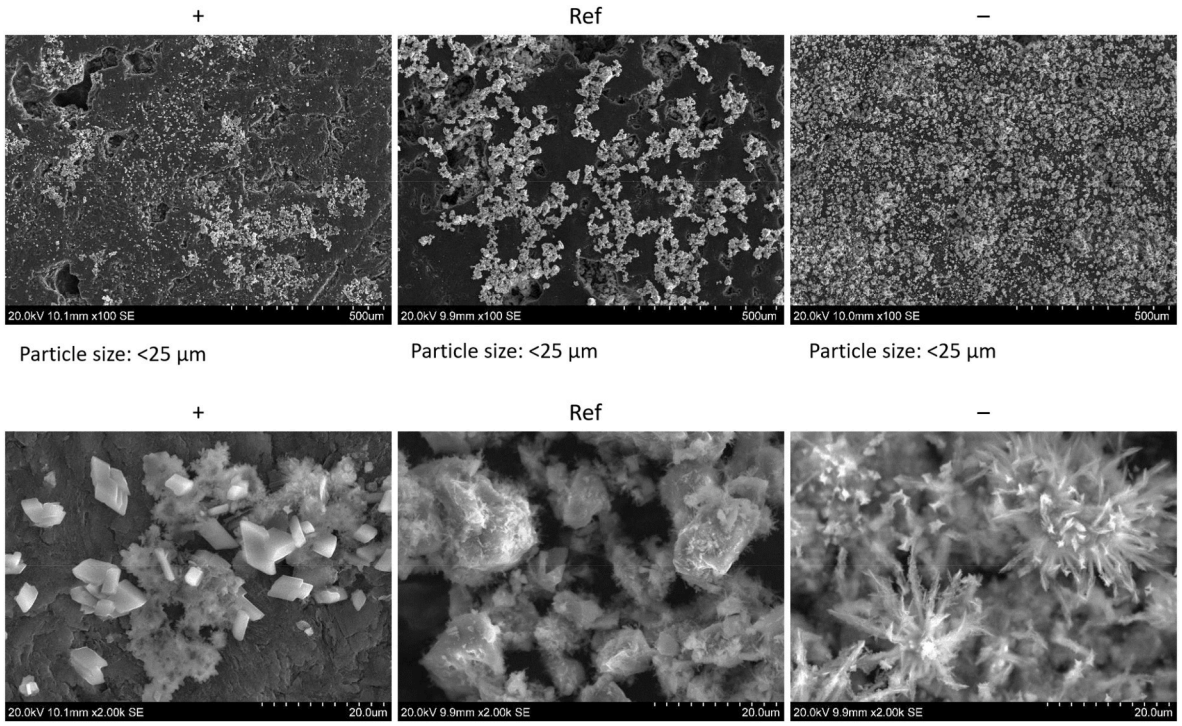

Fig. 5. SEM SE-image of the graphite surfaces, anode (+), cathode (-) and the reference surface (R), after removal from the cement dispersion in water at two different magnifications. The smaller magnification images are representative for particle size distribution while the larger magnification images show particle shape.

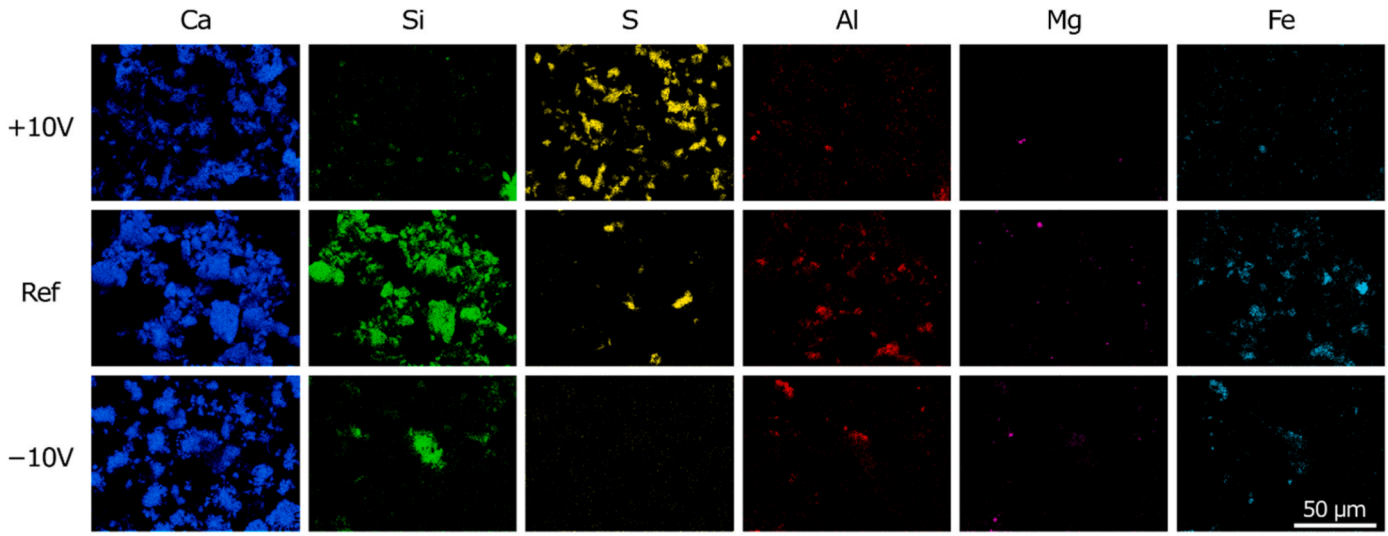

Fig. 6. EDS maps showing elemental composition of cement particles residing on graphite surfaces anode (+), cathode (-) and the reference surface (Ref), after removal from the cement dispersion in water.

Table 3
Atomic composition of particles at electrodes (cathode and anode) as well as the reference sample surface after exposure to cement slurry in water after polarization at 10 V.

at.%	Ca	Si	Al	Fe	Mg	S	Na	P	Cl	K	V	Mn	Ca/Si
+	53.15	12.30	3.00	2.78	1.54	21.86	1.35	0.25	0.50	2.25	0.62	0.38	4.35
ref	65.64	18.76	4.35	4.84	2.80	1.91	0.54	0.10	0.05	0.33	0.05	0.62	3.45
–	76.60	12.00	2.52	2.58	1.96	1.13	1.17	0.17	0.06	1.32	0.10	0.39	6.25

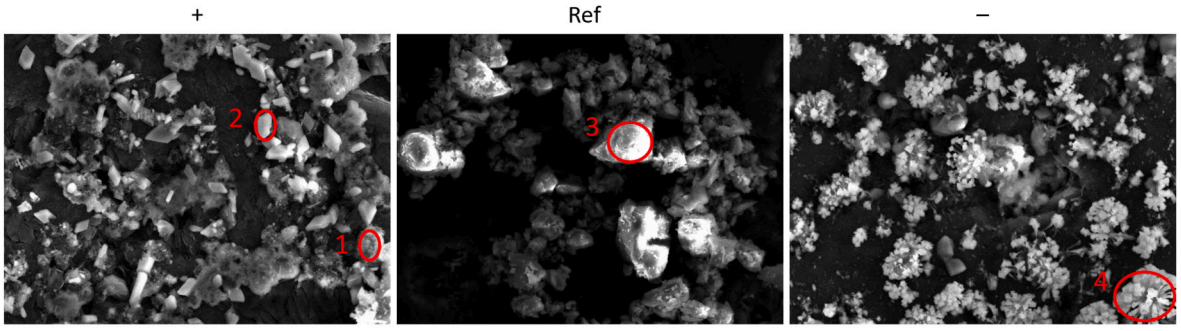

at.%	Ca	Si	Al	Fe	Mg	S	Na	P	Cl	K	V	Mn	Ca/Si	O/Ca	Phase
H2O_plus #1	75.69	8.73	2.01	2.76	1.07	6.78	0.75	0.03	0.29	1.53	0.20	0.17	8.7	3.93	$Ca(OH)_2$ / $CaCO_3$
H2O_plus #2	49.47	4.01	0.79	1.68	0.00	42.02	0.00	0.51	0.12	0.02	0.44	0.94	12.3	8.39	$CaSO_4$
H2O_ref #3	71.76	22.08	1.30	0.20	2.26	0.46	0.85	0.35	0.09	0.19	0.05	0.40	3.2	1.95	Ca_3SiO_5
H2O_minus #4	93.15	4.67	0.59	0.08	0.00	0.89	0.00	0.11	0.19	0.12	0.20	0.00	19.9	3.72	$Ca(OH)_2$ / $CaCO_3$

Fig. 7. SEM images depicting spots, where the EDS spectrum was collected to identify the particle on anode, reference and cathode surfaces, and chemical composition characteristic for the highlighted particle based on EDS data.

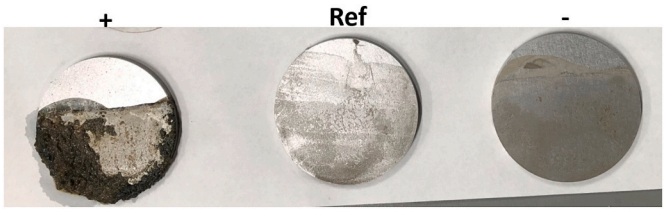

Fig. 8. Photography of steel electrodes: anode (+), cathode (-) and the reference surface (Ref) after removal from the cement dispersion in water.

SEM images in Fig. 9 indicate the presence of scaly precipitate on the anode surface with embedded particles. On the reference surface cement particles with average sizes of around 10–20 μm are present. EDS maps in Fig. 10 and the atomic content data for the material removed from steel electrodes shown in Table 4 suggest that similarly to the graphite electrode, the steel anode surface is rich in sulphur, suggesting an enrichment of sulphate minerals. The material present on the anode electrode is also rich in iron. The iron content is very high in respect to calcium and iron to calcium ratio is significantly higher than in the case of graphite anode.

The XRD data collected from similar experiments performed with

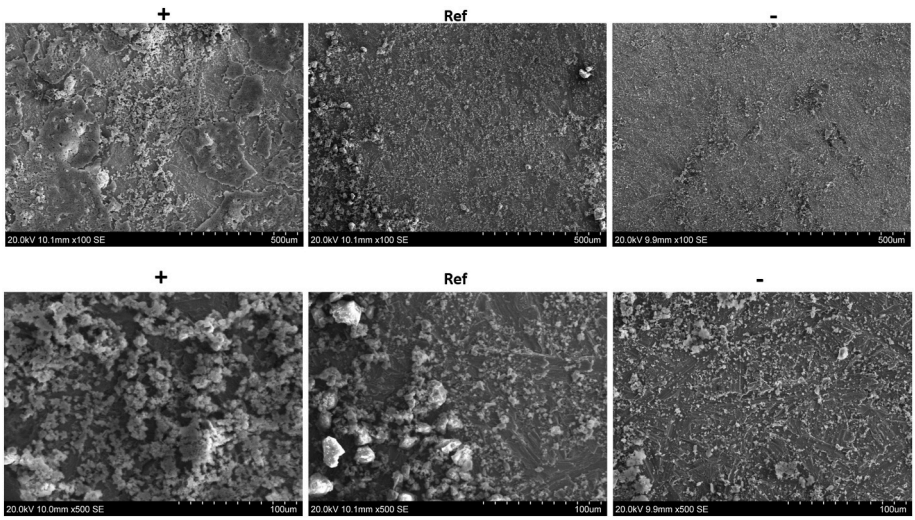

Fig. 9. SEM SE image of the steel surfaces, anode (+), cathode (-) and the reference surface (Ref), after removal from the cement dispersion in water at two different magnifications. The smaller magnification images are representative for particle size distribution while the larger magnification images show particle shape.

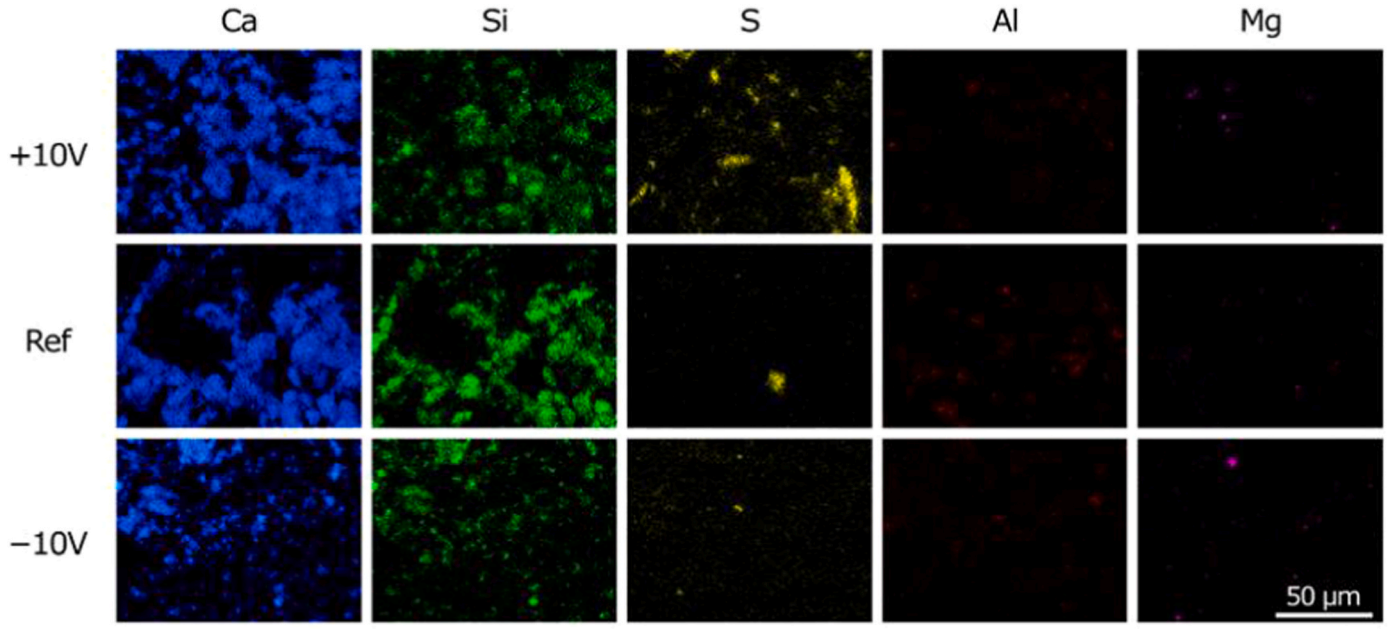

Fig. 10. EDS maps showing elemental composition of cement particles residing on steel surfaces anode (+), cathode (-) and the reference surface (Ref), after removal from the cement dispersion in water.

Table 4
Atomic composition of particles removed from steel electrodes (cathode and anode) as well as the reference steel surface. As the particles for EDS were deposited on SiO_2 wafer O and Si atoms are excluded from calculations.

Atom%	Mg	Al	S	Ca	Fe
+	1	2	15	42	40
Ref	0	9	0	87	4
-	2	6	4	81	8

steel pipes immersed in Portland G cement slurry with identical voltage applied for the same time interval indicate some important differences in the mineralogical composition of hardened cement paste close to the electrode surface (see diffraction patterns in Fig. 11). Namely, gypsum is present in significantly larger quantities at the anode while portlandite is absent on the anode and present on the reference and the cathode surfaces. Portlandite is more abundant on the cathode compared to the reference.

4. Discussion

4.1. Graphite electrodes in 2-propanol

In 2-propanol as a continuous phase of the cement dispersion no chemical changes to cement particles were expected, thus the particles were expected to preserve their original shape and composition. Only physical, electrophoretic processess were expected to affect cement particles in 2-propanol. The largest amount of particles attracted to the negatively polarized electrode in 2-propanol, suggesting that larger amount of cement particles was positively charged in this solvent, and that the positive particles were attracted to the negative electrode as a result of electrophoretic attractive forces in the electric field.

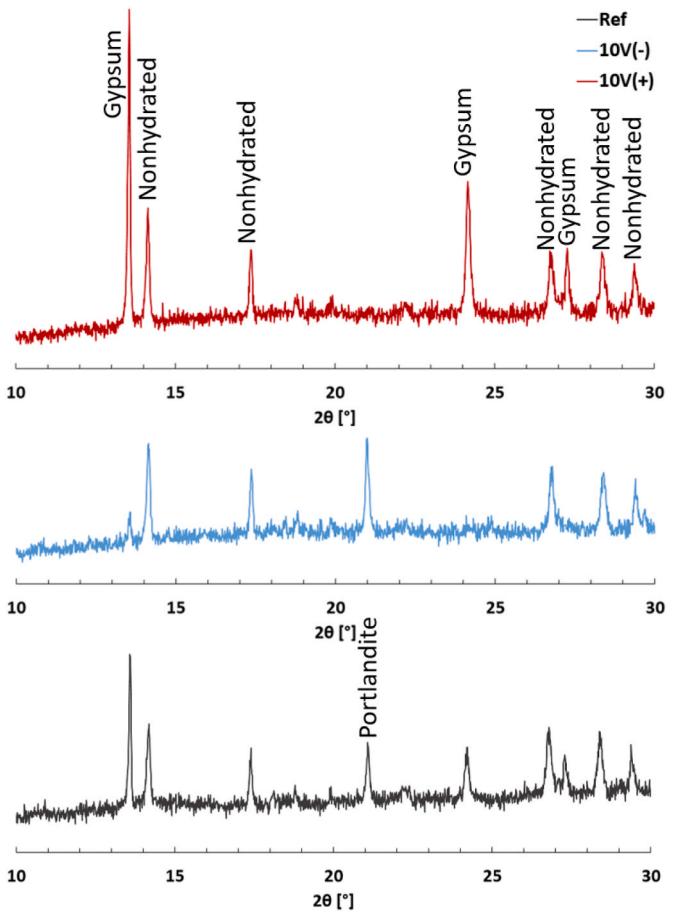

Fig. 11. XRD patterns for cement paste collected from the vicinity of steel surfaces polarized for 1 h at 10 V during cement hardening. Peaks belonging to portlandite, gypsum and nonhydrated cement particles are highlighted.

4.2. Graphite electrodes in water

In aqueous solution as a cement dispersion medium, not only physical electrophoretic phenomena are expected but also chemical and electrochemical reactions. One of the chemical processess occurring in water will be cement hydration reactions. On the other hand, electrochemical reactions associated with water splitting will take place at the applied potential. At the anode oxygen production takes place according to equation (1). This reaction is associated with local decrease of pH close to the anode surface due to simultaneous hydronium production. On the cathode, hydrogen gas is produced according to equation (2). This reaction is associated with local pH increase as co-products of the reaction at cathode are hydroxide ions [18–20].

$$6H_2O \rightarrow O_{2\ (g)} + 4H_3O^+ + 4e^- \quad (1)$$

$$H_2O + 2e^- \rightarrow H_{2(g)} + 2OH^- \quad (2)$$

The local pH changes close to electrodes together with electrophoretic phenomena were expected to affect cement hydration close to graphite surfaces.

Indeed a significant difference in the (1) amount of adsorbed cement particles; (2) morphology of the hydration products and (3) chemical composition of the hydration products was observed between cathode, anode and the reference surface. A large amount of adsorbed material at the cathode (negative electrode) may suggest that large number of cement particles and/or their hydration products had positive surface charge. The adsorption on the graphite anode was significantly limited compared to the cathode and the reference graphite surfaces. This can be associated with the retractive Coulomb forces established between positively charged anode surface and also positively charged cement particles. The acidic environment close to the anode can contribute to dissolution of cement particles and hydration products. It is well established that acidic conditions are degenerative for Portland cement materials [21,22].

The most significant differences in chemical composition between the three graphite surfaces in water found based on EDS analysis (Fig. 7) are: (1) the presence of large amounts of calcium sulphate on the anode surface as well as (2) domination of calcium hydroxide and/or calcium carbonate at the cathode. The carbonation is a rather quick process in air and humid conditions [23], thus the presence of carbonate will be a consequence of carbonation reactions undergoing upon sample drying after cathode removal from the solution.

The presence of calcium hydroxide (later carbonated) at the cathode is likely a result of two phenomena: (1) electrophoresis: positively charged calcium cations migrate towards a negative electrode (cathode) [24] where their concentration increases; and (2) electrolysis: hydroxide ions are produced at the cathode contributing to pH increase. The large amount of calcium cations and hydroxide ions close to cathode result in faster precipitation of calcium hydroxide compared to the reference surface where cement hydration undergoes without being perturbed by electric field and electrolytic reactions. The evidence of similar effects have been previously reported by Lavrov et al. [13] who observed differences in push-out strengths for the electrically polarized and non-polarized steel pipes embedded in Portland G cement paste. Lavrov et al. suggested a hypothesis that portlandite ($Ca(OH)_2$) is preferentially deposited close to the cathode, and this work supplies experimental evidence supporting this hypothesis.

The anode (positive electrode) attracts anions present in the solution [24]. There are two types of anions that are most abundant in cement slurry: hydroxide ions (OH^-) and sulphate ions (SO_4^{2-}). These will migrate towards the anode and their concentration will be increased compared to the reference surface. While hydroxide ions will be (at least partially) neutralized by hydronium ions (produced at anode as a result of water electrolysis), the sulphate ions will react with calcium forming calcium sulphate ($CaSO_4$, gypsum).

The presence of both calcium sulphate and calcium hydroxide at the anode surface suggests that not all hydroxide ions were neutralized, but also contribute to the formation of calcium hydroxide. It must be emphasized that the concentration of hydroxide ions in cement slurry is very high, contributing to pH values of 12–13 [25,26]. Water to cement ratio in such slurries ranges typically between 0.4 and 0.6 while in our case w/c was very high i.e. 6. This high w/c ratio may imply lower pH than 13 but it is still highly alkaline since the equilibrium pH of solid calcium hydroxide is 12.5. Indeed the pH measurements indicated that pH was 12.42.

4.3. Steel electrodes in water

Similar processess as described for graphite electrodes will take place in case of steel electrodes in alkaline solution [27]. In addition carbon steel will undergo corrosion under anodic polarization at the high potentials used here. The presence of green deposits on the steel anode surface suggests the presence of steel corrosion products. In corrosion chemistry there exist a term "Green rust". The term encompasses various green chemical compounds being a corrosion products of divalent iron containing materials. From chemical point of view, the green rust contain iron (II)) cations and it may contain: hydroxide (OH^-) carbonate (CO_3^{2-}), chloride (Cl^-), or sulphate (SO_4^{2-}) anions depending on their availability [28]. In the cement slurry one can expect mainly hydroxide and sulphate anions although chloride and carbonate ions may also be present in smaller amounts (less than 0.1%). It is thus highly likely that the green rust may be formed close to the anode, in the direction of which, the anions from cement slurry migrate in the electric field. Lay et al. reported that the Fe(O)OH colloids (a product of reaction between

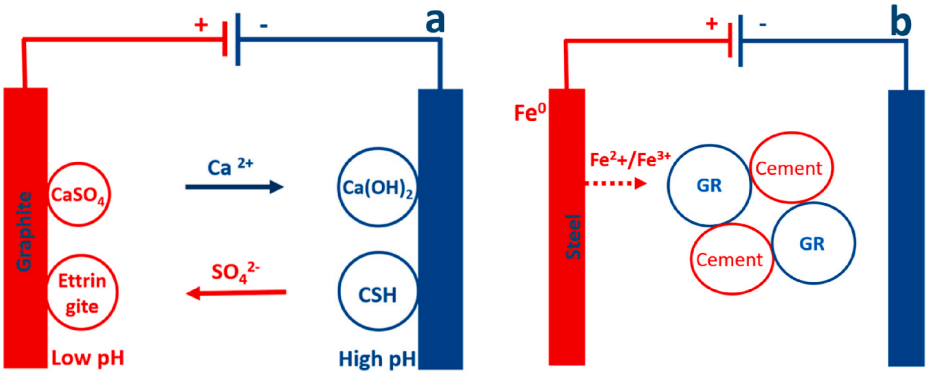

Fig. 12. Schematic representation of cement hydration in electric field between a) graphite electrodes, b) steel electrodes. In case of steel electrodes similar processess as for graphite are expected but for simplicity only phenomena specific for steel are illustrated in Figure b. (GR="green rust" which is steel corrosion product).

ferric iron and water at alkaline conditions) in the presence of sulphate and hydroxide ions show negative zeta potential [29]. On the other hand, cement particles are slightly positively charged which is manifested in their significantly stronger adsorption on the negative electrode. Slightly positive zeta potential of cement particles is also in line with findings reported by others [30] although both positive and negative zeta potentials for Portland cement particles in aqueous suspensions has previously been reported [30–32].

Given the opposite zeta potential of steel corrosion products and cement particles, coagulation in the system can be expected. The large amount of the material adsorbed on the steel anode surface was thus most likely a coagulation product. Fig. 12 depicts schematically the above described phenomena undergoing on steel anode.

The electric field affects abundance of minerals close to the electrically polarized surfaces. The presence of large amounts of calcium sulphate (gypsum) close to anode and larger than in cement bulk amounts of calcium hydroxide may affect setting time, material shrinkage as well as resulting material properties like e.g. porosity, permeability etc.

Gypsum is known as a retarding agent of cement setting time [33]. During hydration gypsum reacts with C3A to generate calcium sulfoaluminate hydrate (ettringite) which forms a protecting film on the cement particles that hinders the hydration of C3A and delay the setting time of cement. On the other hand, too much gypsum may accelerate the setting of cement because gypsum can generate a coagulating agent [33]. The appropriate amount of gypsum depends on the content of C3A in the cement. The large gypsum content may contribute to lower mechanical strength of cement and may cause expansion that may lead to mechanical destruction of cement paste [33].

On the other hand larger amount of calcium hydroxide will accelerate Portland cement early hydration. As a result the early-age strength of cement is increased but later the strength may be adversely affected. Whether or not the later reduction in strength will take place is depend on the cement chemistry, fineness, and presence of siliceous additives like e.g. fly ash.

5. Conclusions

Scanning electron microscopy and energy dispersive X-ray spectroscopy were used to image differences in cement hydration products close to electrically polarized surfaces of graphite and steel. The hydration products present on anode, cathode and the reference surfaces have different structure and atomic composition.

The surface of the graphite anode was abundant in calcium sulphate while the surface of the cathode was almost exclusively covered in calcium hydroxide in addition to calcium silicate hydrate. It has been suggested that the occurrence of large amounts of sulphates close to the anode and calcium close to cathode is due to electrophoretic transport of sulphate and calcium ions towards oppositely charged electrodes. The results for steel electrodes were similar, but in addition, electrochemically induced corrosion on the anode contributed to strong coagulation processes between corrosion products and oppositely charged cement particles.

The compositional changes undergoing in an electric field will affect structure and properties of the resulting materials.

It is likely that similar phenomena may undergo close to the surface of electrically polarized conductive micro and nano-sized fillers in cement composite materials which may allow for new engineering possibilities of these materials.

Declaration of competing interest

The authors declare that they have no known competing financial interests or personal relationships that could have appeared to influence the work reported in this paper.

Acknowledgement

The authors gratefully acknowledge the financial support from: (1) the strategic SINTEF Industry project number 102021203 "Electrophoretic cleaning and friction reduction for applications in drilling and well construction" and (2) The Norwegian Research Council in the form of grant number 285568 "Well fossilization for P&A".

References

[1] K.L. Scrivener, P. Juilland, P.J.M. Monteiro, Advances in understanding hydration of Portland cement, Cement Concr. Res. 78 (2015) 38–56.
[2] J. Cheung, et al., Impact of admixtures on the hydration kinetics of Portland cement, Cement Concr. Res. 41 (12) (2011) 1289–1309.
[3] E.B. Nelson, D. Guillot (Eds.), Well Cementing, Schlumberger, 2006.
[4] J. Beaudoin, I. Odler, 5 - hydration, setting and hardening of Portland cement, in: P.C. Hewlett, M. Liska (Eds.), Lea's Chemistry of Cement and Concrete, fifth ed., Butterworth-Heinemann, 2019, pp. 157–250.
[5] K. Gawel, et al., Study of materials retrieved from a Ketzin CO2 monitoring well, Energy Proc. 114 (2017) 5799–5815.
[6] Y. Liu, et al., Ohmic heating curing of carbon fiber/carbon nanofiber synergistically strengthening cement-based composites as repair/reinforcement materials used in ultra-low temperature environment, Compos. Appl. Sci. Manuf. 125 (2019), 105570.
[7] Y. Liu, M. Wang, W. Wang, Ohmic heating curing of electrically conductive carbon nanofiber/cement-based composites to avoid frost damage under severely low temperature, Compos. Appl. Sci. Manuf. 115 (2018) 236–246.
[8] M. Liebscher, et al., Electrical Joule heating of cementitious nanocomposites filled with multi-walled carbon nanotubes: role of filler concentration, water content, and cement age, Smart Mater. Struct. 29 (12) (2020), 125019.
[9] J.D. McIntosh, Electrical curing of concrete, Mag. Concr. Res. 1 (1) (1949) 21–28.
[10] W. Ding, et al., Roles of CSH gel in the microstructure and piezoelectric properties variation of cement-based piezoelectric ceramic composite, Mater. Lett. 306 (2022), 130952.

[11] W. Ding, et al., Influence of hydration capacity for cement matrix on the piezoelectric properties and microstructure of cement-based piezoelectric ceramic composites, Mater. Char. 179 (2021), 111390.
[12] A. Lavrov, K. Gawel, M. Torsæter, Manipulating cement-steel interface by means of electric field: experiment and potential applications, AIMS Materials Science 3 (3) (2016) 1199–1207.
[13] A. Lavrov, et al., Effect of electric field on push-out strength of cemented steel pipes, AIMS Materials Science 8 (3) (2021) 373–389.
[14] A. Lavrov, et al., Electrophoresis-induced structural changes at cement-steel interface, AIMS Materials Science 5 (3) (2018) 414–421.
[15] D.-Z. Zhu, D.-M. Sun, Q.-S. Wu, Assembly of nano-superstructural aragonite CaCO3 by living bio-membrane, J. Exp. Nanosci. 6 (6) (2011) 622–630.
[16] M. Altiner, M. Yildirim, Production and characterization of synthetic aragonite prepared from dolomite by eco-friendly leaching–carbonation process, Adv. Powder Technol. 28 (2) (2017) 553–564.
[17] M.B. Toffolo, The significance of aragonite in the interpretation of the microscopic archaeological record, Geoarchaeology 36 (1) (2021) 149–169.
[18] L. Edvardsen, et al., Electrochemical enhancement and inhibition of calcium carbonate deposition, J. Environ. Chem. Eng. 8 (5) (2020), 104239.
[19] A. Persat, M.E. Suss, J.G. Santiago, Basic principles of electrolyte chemistry for microfluidic electrokinetics. Part II: coupling between ion mobility, electrolysis, and acid–base equilibria, Lab Chip 9 (17) (2009) 2454–2469.
[20] K. Obata, et al., In situ observation of pH change during water splitting in neutral pH conditions: impact of natural convection driven by buoyancy effects, Energy Environ. Sci. 13 (12) (2020) 5104–5116.
[21] J. Bensted, A. Rbrough, M.M. Page, 4 - chemical degradation of concrete, in: C. L. Page, M.M. Page (Eds.), Durability of Concrete and Cement Composites, Woodhead Publishing, 2007, pp. 86–135.
[22] M.J. McCarthy, T.D. Dyer, 9 - pozzolanas and pozzolanic materials, in: P. C. Hewlett, M. Liska (Eds.), Lea's Chemistry of Cement and Concrete, fifth ed., Butterworth-Heinemann, 2019, pp. 363–467.
[23] M. Samari, et al., Direct capture of carbon dioxide from air via lime-based sorbents, Mitig. Adapt. Strategies Glob. Change 25 (1) (2020) 25–41.
[24] P. Atkins, J. De Paula, Elements of Physical Chemistry, Oxford University Press, USA, 2013.
[25] A. Kenny, pH Measurement in Cement Paste as a Method for Chemical Reactions Analysis, 2007.
[26] B.G. Kutchko, et al., Degradation of well cement by CO2 under geologic sequestration conditions, Environ. Sci. Technol. 41 (13) (2007) 4787–4792.
[27] S. Anantharaj, et al., Stainless steel scrubber: a cost efficient catalytic electrode for full water splitting in alkaline medium, ACS Sustain. Chem. Eng. 6 (2) (2018) 2498–2509.
[28] P. Refait, et al., Corrosion of carbon steel in marine environments: role of the corrosion product layer, Corros.Mater. Degrad. 1 (1) (2020) 198–218.
[29] M.L. Lay, H.M. Wu, C.H. Huang, Study of the zeta potential of Fe(O)OH colloids, J. Mater. Sci. 30 (21) (1995) 5473–5478.
[30] S. Srinivasan, et al., Characterising cement–superplasticiser interaction using zeta potential measurements, Construct. Build. Mater. 24 (12) (2010) 2517–2521.
[31] R.J. Flatt, C.F. Ferraris, Acoustophoretic characterization of cement suspensions, Mater. Struct. 35 (9) (2002) 541–549.
[32] J.-Y. Shih, T.-P. Chang, T.-C. Hsiao, Effect of nanosilica on characterization of Portland cement composite, Mater. Sci. Eng., A 424 (1) (2006) 266–274.
[33] *4* - cement, in: H. Zhang (Ed.), Building Materials in Civil Engineering, Woodhead Publishing, 2011, pp. 46–423.